Differential permissivity of human cerebrovascular endothelial cells to enterovirus infection and specificities of serotype EV-A71 in crossing an in vitro model of the human blood–brain barrier

Romain Volle, Christine Archimbaud, Pierre-Olivier Couraud, Ignacio Romero, Babette Weksler, Audrey Mirand, Bruno Pereira, Cécile Henquell, Hélène Peigue-Lafeuille, Jean-Luc Bailly

JGV Papers in Press. Published February 23, 2015 as doi:10.1099/vir.0.000103

Journal of General Virology

Differential permissivity of human cerebrovascular endothelial cells to enterovirus infection and specificities of enterovirus 71 in crossing an in vitro model of human blood brain barrier

--Manuscript Draft--

Manuscript Number:	VIR-D-14-00304R1
Full Title:	Differential permissivity of human cerebrovascular endothelial cells to enterovirus infection and specificities of enterovirus 71 in crossing an in vitro model of human blood brain barrier
Short Title:	Impairment of the blood brain barrier by enteroviruses
Article Type:	Standard
Section/Category:	Animal - Positive-strand RNA Viruses
Corresponding Author:	Jean-Luc Bailly, PhD Clermont Université Clermont-Ferrand, FRANCE
First Author:	Romain Volle
Order of Authors:	Romain Volle
	Christine Archimbaud
	Pierre-Olivier Couraud
	Ignacio A. Romero
	Babette Weksler
	Audrey Mirand
	Bruno Pereira
	Cécile Henquell
	Hélène Peigue-Lafeuille
	Jean-Luc Bailly, PhD
Abstract:	Human cerebral microvascular endothelial cells (hCMEC/D3 cell line) form a steady polarized barrier when cultured in vitro on a permeable membrane. Their susceptibility to enterovirus (EV) strains was analysed to investigate how these viruses may cross the blood-brain barrier. A sample of 88 virus strains was selected on phylogenetic features among 44 epidemiologically relevant types of the four EV species A-D. The EV-A71 genome was replicated at substantial rates while the infectious virus was released at extremely low but sustained rates at both barrier sides for at least 4 days. EV-A71 antigens were detected in a limited number of cells. The properties of the endothelial barrier (structure and permeability) remained intact throughout infection. The chronic EV-A71 infection was in sharp contrast with the productive infection of cytolytic EVs (e.g. echoviruses 6 and 30). The hCMEC/D3 barriers infected with the latter EVs exhibited elevated proportions of apoptotic and necrotic cells, which resulted in major injuries to the endothelial barriers with dramatic increase of paracellular permeability and virus crossing to the abluminal side. The following intracellular rearrangements were also seen: early destruction of the actin cytoskeleton, remodelling of intracellular membranes, and reorganization of the mitochondrion network in a small cluster near the perinuclear space.

Title

Differential permissivity of human cerebrovascular endothelial cells to enterovirus infection and specificities of enterovirus 71 in crossing an in vitro model of human blood brain barrier

Authors

Romain Volle[1,2], Christine Archimbaud[1,2], Pierre-Olivier Couraud[4], Ignacio A. Romero[5], Babette Weksler[6], Audrey Mirand[1,2], Bruno Pereira[3], Cécile Henquell[2], Hélène Peigue-Lafeuille[1,2], and Jean-Luc Bailly[1,2*]

Affiliations

1 Clermont Université, Université d'Auvergne, EPIE, EA 4843, Clermont-Ferrand, France

2 CHU Clermont-Ferrand, Service de Virologie, Clermont-Ferrand, France

[3] CHU Clermont-Ferrand, DRCI, Clermont-Ferrand, France

[4] Inserm, U1016, Institut Cochin, Paris, France

[5] Department of Life, Health and Chemical Sciences, Open University, Milton Keynes, U.K

[6] Weill Cornell Medical College, New York, NY, USA

Running title

Impairment of the blood brain barrier by enteroviruses

Word counts: Abstract, 203; Main text, 5429

Correspondent footnote: Jean-Luc Bailly

Phone: +33 4 73 17 81 42; Fax: +33 4 73 75 48 51; j-luc.bailly@udamail.fr

ABSTRACT

Human cerebral microvascular endothelial cells (hCMEC/D3 cell line) form a steady polarized barrier when cultured *in vitro* on a permeable membrane. Their susceptibility to enterovirus (EV) strains was analysed to investigate how these viruses may cross the blood-brain barrier. A sample of 88 virus strains was selected on phylogenetic features among 44 epidemiologically relevant types of the four EV species A–D. The EV-A71 genome was replicated at substantial rates while the infectious virus was released at extremely low but sustained rates at both barrier sides for at least 4 days. EV-A71 antigens were detected in a limited number of cells. The properties of the endothelial barrier (structure and permeability) remained intact throughout infection. The chronic EV-A71 infection was in sharp contrast with the productive infection of cytolytic EVs (**e.g.** echoviruses 6 and 30). The hCMEC/D3 barriers infected with the latter EVs exhibited elevated proportions of apoptotic and necrotic cells, which resulted in major injuries to the endothelial barriers with dramatic increase of paracellular permeability and virus crossing to the abluminal side. The following intracellular rearrangements were also seen: early destruction of the actin cytoskeleton, remodelling of intracellular membranes, and reorganization of the mitochondrion network in a small cluster near the perinuclear space.

INTRODUCTION

Enteroviruses (EVs; *Picornaviridae*) form a large group of non-enveloped enteric viruses, of which more than 100 different serotypes are human pathogens classified within four taxonomic species (EV-A to EV-D). Human EVs are transmitted through faecal-oral and respiratory routes and they actively replicate in the mucosa and epithelial cells of the throat and intestinal tract. Viral invasion of the intravascular space or viremia may result in spreading to sites such as the skin, heart and central nervous system (CNS).

The most common clinical manifestation associated with CNS EV infections is aseptic meningitis. Encephalitis, cerebellitis, myelitis, and poliomyelitis are also observed but less frequently (Khetsuriani *et al*., 2006; Antona *et al*., 2007). There is evidence for hematogenous and neural routes of poliovirus (PV) dissemination and both involve viremia (Sabin, 1956); the two routes are not mutually exclusive. By the neural pathway, it is suggested that the virus is conveyed by retrograde axonal transport from infected tissues to the CNS via peripheral nerves (Ren & Racaniello, 1992; Gromeier & Wimmer, 1998). In mouse models, PV can be transported along nerves through either a process involving the CD155 receptor or a receptor-independent manner (Okha *et al*., 2012). Investigations with different animal models have revealed a possible link between neurological injury caused by enterovirus A71 (EV-A71) and retrograde axonal transport of the virus to the CNS (Chen *et al*., 2007; Khong *et al*., 2012). The occurrence of encephalomyelitis and subsequent paralysis associated with these two EVs could be explained by transport via the neural pathway but the inefficiency of the axonal transport limits virus access to the CNS (Lancaster & Pfeiffer, 2010).

Alternatively, a virus in the bloodstream may enter the CNS by crossing the vascular endothelium in the meninges, the choroid plexus, or the brain parenchyma. PV-1 was suggested to cross the mouse blood-brain barrier (BBB) independently of the CD155 receptor

and of infected leucocytes (Yang *et al*., 1997). During EV-A71 infection, viremia early after the onset of disease was related to severe CNS involvement in young children (Cheng *et al*., 2014) and to neurological impairment in experimentally infected rhesus monkeys (Zhang et al., 2011). In neonates infected with coxsackievirus B3 (CV-B3), a high blood viral load was related to greater disease severity (Yen *et al*., 2007). Using sensitive quantitative gene amplification techniques to amplify viral RNA from the cerebrospinal fluid (CSF), it is possible to detect evidence of EV infection of the CNS in patients with aseptic meningitis early after the onset of disease in both children and adults (Volle et al., 2014). Our current knowledge about the processes involved in EV immigration into the CSF is still limited. As this inflammatory disease of the subarachnoid space is common to most EV serotypes, it is assumed that viruses travel through the blood, breaching the blood-CSF barrier either directly or through infected leukocytes. A number of studies showed that PV, CV-B3, and EV-A71 can infect various immune cells (Eberle *et al*., 1995; Vuorinen *et al*., 1996; Haddad *et al*., 2004; Wahid *et al*., 2005a; 2005b; Tabor-Godwin *et al*., 2010). These data suggest a role of infected leukocytes in EV dissemination to the CNS through a "Trojan-horse" process. In vitro studies showed the susceptibility to different EVs of human vascular endothelial cells of different tissue origins (Conaldi *et al*., 1997; Ylipaasto *et al*., 2010; Saijets *et al*., 2003; Liang *et al*., 2004; Zanone *et al*., 2003; Bozym *et al*., 2010). In addition, PV-1 and CV-B3 induce different cell signalling and endocytosis pathways in human brain microvascular endothelial cells (HBMEC), which is suggestive of possible variations in BBB crossing between EV types (Bozym *et al*., 2010; Coyne *et al*., 2007).

In this study we used the human cerebral microvessel endothelial cell line D3 (hCMEC/D3) as a model of brain endothelium (Weksler *et al*., 2005; 2013). The hCMEC/D3 cells were used as a model for investigating whether or not EVs can breach an endothelial

barrier. We first examined the susceptibility of hCMEC/D3 cells to infection by a set of 44 EV serotypes and then analysed the ability of a subset of EVs to cross endothelial barriers.

RESULTS

Susceptibility of hCMEC/D3 cells to 44 EV types. We used a first set of 88 virus strains (**Table S1**) chosen within species B (EV-B; n=37 types), EV-A (n=5), EV-C (n=1), and EV-D (n=1). Susceptibility of hCMEC/D3 cells to EV strains was assessed in duplicate at 24 h p.i. by measurement of the production of viral RNA and infectious virus (**Fig. S1)**. The virus yield exhibited a positive correlation (Spearman's rho 77%, p-value <0.001) with viral RNA production **(Fig. 1a)**. The virus strains selected among the EV-B types displayed different replication patterns defined by two arbitrarily selected thresholds of 0.00 $\log_{10}$ infectious particles and 3.00 $\log_{10}$ genome copies per cell. The highest infectivity rates (from –0.55 to 2.86 $\log_{10}$ infectious particles per cell and 2.12 to 5.53 $\log_{10}$ genome copies per cell) were determined for the epidemiologically infrequent types echovirus 1 (E-1) and EV-B69 and the epidemic types E-6, E-11, E-12, E-13, and E-30. The strains selected among CV-B and EV-A types displayed the lowest infectivity rates (respectively, from –2.89 to 0.01 and –2.38 to –0.41 $\log_{10}$ infectious particles per cell, and –0.44 to 3.53 and 2.01 to 4.51 $\log_{10}$ genome copies per cell).

Kinetics of viral RNA production performed in triplicate for EV-A71, E-6, E-30, and E-12 strains showed the highest rates of virus replication between 2 and 6 h p.i. (p-value 0.001; **Fig. 1b)**. Different peaks of viral RNA production were reached at 24 h p.i. among the viruses tested (mean±SD in $\log_{10}$ copies per cell): EV-A71 (3.29±0.58), E-30 (4.15±0.30), E-6 (5.30±0.25), and E-12 (5.56±0.21). These RNA levels were consistent with those obtained in **Fig. 1a**: 2.46±0.63, 3.85±0.26, 5.02±0.15, and 5.46±0.15, respectively.

We determined the number of infected cells at 6 h p.i. (before extensive release of virus progeny) to investigate whether the variations in susceptibility of hCMEC/D3 cells were related to differences in the infection efficiencies of EV strains. The infected cells were numbered in triplicate by computer-assisted image processing of low magnification

epifluorescence pictures. The highest proportion of infected cells (>30%) was determined for E-19, EV-B69, and E-1, and intermediate proportions of 10–30% were obtained with E-12 and E-16 (**Fig. 1c**). Less than 10% of infected cells were counted for virus strains of various types (E-30, E-3, E-7, CV-B6, E-4, E-14, E-18, EV-A71, E-9, E-32, CV-B3, and E-25). About 20 infected cells per cm² were counted for E-27 and E-11, and only 3–5 infected cells per cm² for EV-B70, EV-B77, CV-A9, E-15, E-24, and E-26 (data not shown). Two E-6 and E-13 strains exhibited different infection efficiencies (E-6/CF2660-01 >30%; E-6/CF158061-11 and E-13/CF1275-00 10–30%; E-13/CF1925-01 <10%). The overall data suggest variations in the susceptibility of the hCMEC/D3 cells to infection by different EV types and subtypes.

Cell mortality during virus infection and multidimensional analysis of EV infectivity. The mortality rates of infected hCMEC/D3 cells were determined in quadruplicate at 24 h p.i. for a subset of 15 EV strains representative of different susceptibility patterns determined above in hCMEC/D3 cells **(Fig. 1d)**. The mortality threshold was defined by the highest value of the standard deviation calculated with mock infected cells (i.e. 10%). High cell mortality rates >50% were found with E-1 and EV-B69, and cell death resulted from both necrosis and apoptosis. Intermediate cell mortality rates between 40 to 50% were estimated for E-12, E-6/CF2660-01, and E-30/CF282-97. Other virus strains of the two latter types caused lower cell mortality (30–40%). Two E-13 strains were related to different cell mortality rates (CF1274-00, 38.3%; CF1925-01, <30%). Mortality of cells infected with EV-A71 (11%) was similar to that of mock infected cells.

We used principal component analysis (PCA) to visualize on a map the ordination of the 15 EV strains according to the proportion of infected cells, the production of viral genomes, the yield of infectious particle production, and cell mortality rates (**Fig. S2**). The

proportion of infected cells and cell mortality exhibited a positive correlation, hereafter designated cell sensitivity (x-axis). The productions of viral genomes and infectious virus were positively correlated and designated as viral replication (y-axis). As cell sensitivity and viral replication were orthogonal, they were not correlated with each other. PCA confirmed that the hCMEC/D3 cell line displayed large differences in sensitivity to EV types and strains within the same type (**Fig. 2**). We selected viral strains representative of different PCA patterns for further investigations with endothelial barriers (Table S2).

Variations in permeability and structural integrity of endothelial barriers among EV types. We prepared endothelial barriers *in vitro* with the hCMEC/D3 cells (see **Fig. S3**) and quantified infection with five EV types so that infection and paracellular permeability were assessed in the same samples. The structural features of mock-infected endothelial monolayers and their restrictive permeability were analysed with transmission electron microscopy (TEM) and clearance of a non-permeable fluorescent compound (**Figs. S3 and S4)**. Endothelial barriers infected with E-6, E-11, E-12, and E-30 strains exhibited little change in paracellular permeability at 24 h p.i. but permeability progressively increased afterwards (**Fig. 3a–3d**). A release of viral genomes (>6 $\log_{10}$ copies) was detected at 6 h p.i. at both barrier sides, but in the abluminal compartment, viruses were detectable below the titration threshold for E-12 and E-30. The release of infectious progeny reached highest levels at 24–48 h p.i. Scanning electron microscopy (SEM) allowed the identification of three main cytological alterations (**Fig. 4**). Compared to mock infected controls, which had the appearance of joined cobblestones (**Fig. 4a–4c)**, the infected endothelial barriers exhibited cells with structural features suggestive of necrosis (damage plasma membrane) and apoptosis (preserved and budded plasma membrane), indicated, respectively, by red and green arrow heads in **Fig. 4d–4l**. Rounded cells without apparent altered plasma membrane

were suggestive of early steps of cell death (see blue arrow heads). On the basis of these analyses, we found evidence of large amounts of altered cells, which caused breaches within endothelial barriers, as indicated by the visualization of pores of the microporous membrane (white arrow heads).

The paracellular permeability of endothelial barriers infected with the EV-A71 strains (genogroups C1 and C2) was maintained at levels similar to those of mock-infected barriers until 96 h p.i. (**Fig. 3e and 3f)**. The abluminal release of EV-A71 genomes and infectious virus was highest at 24 h p.i. and remained constant at slightly lower levels up to 96 h p.i. The infectious progeny was below the titration threshold at the abluminal side after 24 h p.i., but was consistently determined at low levels at the luminal side. SEM observations showed few groups of infected cells and a limited number of small breaches (**Fig. 4m–4o**).

Intracellular changes in endothelial barriers during EV infection. The endothelial barriers were analysed by TEM to visualize the intracellular features of infected hCMEC/D3 cells and to investigate variations between EV types. The altered cells of endothelial barriers infected with the E-6/CF2660-01 strain displayed features indicative of virus infection, which were similar to those caused by E-30 and E-12 (data not shown). At 24 h p.i., the impaired cells displayed shrunken nuclei relocated near the cell membrane and contained myriads of virus-induced vesicle-like membranous structures, 200 nm in diameter (**Fig. 5a and 5b)**. These structures had either single or double membranes and were organized in extensive intracellular arrangements (**Fig. 5c**). Some infected cells showed evidence of tubular structures with positive membrane invagination that enclosed cytoplasmic components (**Fig. 5d).** Clusters of electron-dense granules between membranous structures were suggestive of viral particles (**Fig. 5e**). Mitochondria were grouped near the membranous structures, which contrasted with mock-infected cells, in which mitochondria formed an extensive network

(**Fig. S4**). Large single-membrane vesicles (600−1000 nm in diameter) contained electron-dense cytoplasmic material and multilamellar structures resembling autophagic vacuoles (**Fig. 5c**).

In contrast to the features described above, the impaired cells of endothelial barriers infected with EV-A71/CF166105-10 displayed a number of structural variations. As shown in **Fig. 6a–6d**, the EV-A71 infected cells maintained an elongated shape and contained nuclei similar in shape to those seen in control barriers. Remodelling of intracellular components included vesicle-like structures and mitochondria clustered near the nucleus whereas EV-A71-induced membranous structures had a uniform round shape with a diameter of 500 nm and a multilamelar structure (**Fig. 6e–6i**).

Intracellular injury patterns common to EV types. The early virus-induced intracellular injuries at 6 h p.i. were further analysed by confocal microscopy and viral replication was detected by staining the VP1 protein. The infected cells displayed major reduction in staining of polymerized actin in comparison to controls (**Fig. 7a–7r vs Fig. 7s–7u)**. This indicates effective cytoskeleton impairment early after the initiation of viral protein synthesis and would explain the subsequent cell rounding.

Early virus-induced changes in the mitochondrion network were analysed with a fluorescent probe that accumulates in active mitochondria. Mitochondria were stained in all virus-infected cells (**Fig. 8a–8o**) but, in contrast to mock-infected controls, they were clustered in a perinuclear area (**Fig. 8p–8r**). Rearrangement of the mitochondrion network was marked in cells exhibiting prominent staining of the VP1 protein at 6 h p.i. (see white arrowheads). Cells with reduced VP1 staining exhibited no or minor changes in the mitochondrion network (see yellow arrowheads). Mitochondrion clustering was dependent on

viral replication intensity but was not directly related to cell rounding, since cells that were not yet round were also displaying clustered mitochondria.

DISCUSSION

Human EV infections are associated with meningitis, encephalitis, and encephalomyelitis but our current knowledge about CNS invasion by enteric viruses is still scant. The BBB may represent a common entry pathway for EVs during viremia, which precedes disease onset. In this study, we used the human cerebral microvascular endothelial cell line hCMEC/D3 as a model system for investigating EV entry routes into the CNS through the human BBB. We showed that the hCMEC/D3 cells were permissive to infection by a large array of EVs and found major differences between types and genogroups. Most EV strains occupied a central position in the susceptibility spectrum of hCMEC/D3 cells, notably the E-6, E-13, and E-30 strains, and intratypic variations may be related to individual genetic differences among genogroups and subgenogroups. A wide range of cellular receptors has been observed in human EVs (reviewed in Merilahti *et al*., 2012). Although we did not examine the binding processes of EVs to the hCMEC/D3 cell surface, there is a large body of earlier experimental evidence to suggest that the intertypic variations in hCMEC/D3 susceptibility to EVs can be attributed to their propensity for using a wide range of receptors and internalization processes (Ylipaasto *et al*., 2010; Coyne *et al*., 2007; Bozym *et al*., 2010). For instance, E-1 stands apart within the susceptibility spectrum of hCMEC/D3 cells to EV infection, a pattern which may be related to the fact that it is the only type known to bind integrin α2β1 (Bergelson *et al*., 1993). A number of EV types examined in our study (E-6, E-11, E-12, E-13, and E-30) bind the same cellular receptor CD55 (Bergelson *et al*., 1995). Yet, the virus strains of these types did not cluster in the same area of the susceptibility spectrum of hCMEC/D3 cells. This suggests that additional factors other than canonical receptors should be considered and that genogroup features may be involved.

Our investigation provides evidence of two major clusters among EV types. A first cluster consists of the EVs that exhibit a highly cytolytic phenotype, produce infectious

243 progeny, and induce extensive disruption of the endothelial barrier. Early during cellular
244 infection by these viruses, the amount of virus genomes released in the abluminal
245 compartment was >10,000 times higher than that of infectious progeny. We assumed that
246 paracellular transport of viral RNA and defective virus particles was not involved because
247 barrier permeability to the fluorescent reporter was not yet compromised at this time, a
248 hypothesis that is also supported by SEM observations. At 24 h p.i., the difference between
249 the release of viral genomes and virus particles was substantially reduced at the abluminal
250 side as a result of the destruction of the endothelial barrier caused by infected dying cells. In
251 contrast, the release of genomic material was relatively constant over time at the luminal
252 sides. Accordingly, massive amounts of viral genomes appeared to drain off the cells through
253 their basolateral membrane early during infection by a yet unknown process.

254 The second cluster comprises CV-B and EV-A71 types, which produced no
255 impairment of the *in vitro* model of endothelium barrier. A key observation, in sharp contrast
256 with the above data, is that hCMEC/D3 cells are moderately permissive to EV-A71 infection.
257 This pattern resulted from a high replication rate of the viral genome but a remarkably poor
258 production of infectious viruses. Both the virus and viral RNA were released from the
259 luminal and basolateral sides of the endothelial barrier but at disproportionately different
260 rates as the infectious virus was consistently detected at minute amounts. This process was
261 maintained for at least 4 days and did not induce a breakdown of the barrier nor changed the
262 paracellular permeability as measured with the LY surrogate marker. This non-disruptive
263 pattern occurred even when the barriers were inoculated with a MOI of about 100 $TCID_{50}$ per
264 cell (data not shown), which suggests that it was not dependent on the initial infection
265 conditions but was more probably related to post-entry factors. A non-disruptive and long-
266 term replication pattern was also shown for CV-B3 and CV-B5 (data not shown). A
267 persistent replication was reported earlier for CV-B3 and CV-B4 in human dermal

microvascular endothelial cells (Zanone *et al*., 2003). A flavivirus West Nile virus can cross *in vitro* BBB models by infection of endothelial cells (Verma *et al*., 2009). The brain endothelium crossing and infection by West Nile virus is not related to direct disturbance of the endothelial barrier integrity *in vitro*, as observed in our study for EV-A71 and CV-B. The loss of BBB integrity associated with the West Nile virus may be related to up regulation of cell adhesion molecules (e.g. VCAM-I, E-Selectin) in infected endothelial cells, thus promoting trans endothelial migration of leucocytes (Verma *et al*., 2009; 2010).

The infected cells showed typical ultrastructural features of a picornavirus infection. We found evidence for both apoptosis and necrosis among infected cells regardless of the EV type, in agreement with data indicating a competition between cell death pathways and picornavirus replication (Agol & Gmyl, 2010). We also observed disruption of the actin cytoskeleton network and that of intercellular junctions as evidenced by the rounding of infected cells. The actin cytoskeleton has an important role in the maintenance of stable inter endothelial junctions and prevents paracellular transport to the brain (Stamatovic *et al*., 2012; Spindler & Hsu, 2012). Remodelling of intracellular membranes was the third hallmark of a picornavirus infection seen in infected hCMEC/D3 cells but discrete variations occurred between echoviruses (E-6, E-12, and E-30) and EV-A71. In the echovirus infections, we found evidence of single and double membrane vesicles organized in compact arrangements near the nucleus and of structures that displayed positive membrane invagination. Both features were reported earlier in Vero and Hela cells infected by CV-B3 and PV-1, respectively (Limpens *et al*., 2011; Belov *et al*., 2012). The vesicular structure in the EV-A71 infected hCMEC/D3 cells was characterised by less condensed vesicles and an increased proportion of multilamellar and large vesicles. Finally, our analyses with TEM and fluorescence microscopy showed clustering of the mitochondrion network, a previously unobserved feature of EV infections that occurred early during the virus infection and whose

origin is still unclear. It may be related to virus-induced disruption of microtubules, as suggested for cells infected with the hepatitis B virus (Kim *et al*., 2007). A similar feature was also reported for African swine fever virus, another DNA virus, and was related to coupling between viral translation and ATP synthesis (Rojo *et al*., 1998).

The most frequent EV infections of the CNS cause meningitis as a result of virus replication in the cells of the leptomeninges, the brain coverings (**Rotbart, 1995**). These infections are usually self-limited because the meninges are directly accessible to immunologic surveillance and subject to rapid immune responses (**Engelhardt & Coisne, 2011**). The varying amounts of viruses in the CSF of patients with EV meningitis within few hours after the onset of symptoms (**Volle et al., 2014**) may reflect virus unloading from these infected sites. The meningeal blood vessels, which form the barrier between blood and CSF, are only made of non-fenestrated endothelial cells; this contrasts with the BBB, which includes other cell types. Accordingly, our endothelium model is consistent with the blood-CSF barrier. The infection of endothelial cells reported in this study for a large array of EV types may occur during the earliest stages of viremia, which develops following EV replication in peripheral tissues. The local EV replication may contribute to infection of leptomeninges and development of a neuro-inflammatory disease. Of note, regional blood flow reduction and cerebral vasculitis can be observed in children with E-30 aseptic meningitis (**Nishikawa et al., 2000**). Care must be taken in making generalised conclusions of pathophysiology based on *in vitro* model systems and the transcellular passage for neural spread of EVs requires close examination in an appropriate in vivo model.

MATERIALS AND METHODS

Cell lines and viruses. HCMECs were grown in EBM-2 basal medium (Lonza) supplemented with 5% fetal bovine serum (FBS), 1% penicillin (10,000U), 1% streptomycin (10mg/ml; GE Healthcare Life Science), 1% chemically defined lipid concentrate (Invitrogen), 10 mM of HEPES, 1.4 µM of hydrocortisone (Sigma Aldrich), 1.5 $\mu g \times ml^{-1}$ of ascorbic acid (Sigma Aldrich), and 200 $ng \times ml^{-1}$ of basal fibroblast growth factor (Sigma Aldrich). The cells were seeded for all experiments on rat collagen I-coated culture surfaces (RD-System). The rabdomyosarcoma (RD) cells were grown in RPMI 1640 medium (Lonza) with 1% penicillin/streptomycin, and 4% FBS. The buccal epithelial carcinoma (KB) cells were grown in DMEM basal medium (GE Healthcare Life Science) with 1% penicillin/streptomycin, and 6% FBS. All cell cultures were maintained at 37°C in a humidified atmosphere containing 5% CO_2.

A sample of 88 EV strains, comprising 23 reference strains and 65 clinical isolates, recovered from patient specimens (CSF, stool or throat) was used in the study (**Table S1**). Virus stocks were prepared with KB (coxsackievirus B) and RD cells (other EVs) and stored at –20°C. Titration of viral suspensions was done using our end point dilution assay (Bailly *et al*., 1991). The cell cultures were inoculated at a multiplicity of infection (MOI) of 5 for 1 h at 37°C in all experiments; after washing with PBS, they were incubated for the indicated times.

Extraction of nucleic acids and EV real-time RT-qPCR. Nucleic acids were extracted from 200 µl from supernatants or the whole cells and supernatant using the NucliSens®EasyMAG™ extractor (bioMérieux) and were eluted with 25 µl of the elution buffer provided by the manufacturer. A previously described competitive internal control was added during the extraction step and amplified in our in-house RT-qPCR assay (Volle *et al*., 2012).

Viability of infected hCMEC/D3 cells. Cells were infected separately by 15 EV strains. After two washes at 24 h p.i., the cells were detached, centrifuged for 10 min at 1000g, stained with the Apoptotic/Necrotic/Healthy Cells Detection Kit (Promokine), and analysed by flow cytometry (BD-LSRII, BD Bioscience). Cells were considered as being viable when only stained with the Hoechst compound, apoptotic when only stained with the Annexin V conjugated antibody, or necrotic when they were stained with both Annexin V and ethidium homodimere III. Cell fragments were detected through ethidium homodimere III staining alone.

Fluorescent microscopy. HCMEC/D3 cells were grown in chamber slides, infected for 6 hours by different EV strains, and fixed with 4% paraformaldehyde for 10 min. For mitochondria staining, the cells were incubated at 37°C for 1 h before fixation, with complete EBM-2 medium containing 50 nM of MitoTracker® Mitochondrion-Selective probe M7510 (Invitrogen) in a humidified atmosphere of 5% CO_2. Cells were permeabilized with 0.5% Triton X100 in PBS for 5 min, saturated for 10 min with 5% BSA in PBS, and incubated overnight at 4°C with mouse primary monoclonal antibodies against the EV capsid protein VP1 (Diagnostic Hybrid). After three PBS washes, incubation was pursued for 1 h at 37°C in a solution of anti-mouse secondary antibodies conjugated to Dyelight488 (Anticorps enligne). In the tests for which active mitochondria staining was not required, red-phalloïdin used for actin staining was included in the secondary antibody solution. After three PBS washes, nuclear DNA was counterstained with a Hoechst solution (Promokine). The slides were mounted with coverslips and observed with an epifluorescence microscope (Olympus BX41) or scanning confocal microscope (LSM 510, Carl Zeiss MicroImaging Inc.). Automated image analysis (FIJI software) was used to calculate the number of infected cells.

EV crossing through an *in vitro* model of brain microvascular endothelial barrier. To obtain microvascular endothelial barriers, hCMEC/D3 cells were cultured on a permeable

membrane (0.4 µm pore) placed in the upper chamber of a Transwell® device (12-well plate, Corning). The upper chamber was seeded with 40,000 cells/cm² and incubated for 5 to 7 days to obtain a tight confluent cell monolayer. In this *in vitro* model, the cells are polarized and display a luminal side and an abluminal side (Weksler *et al*., 2005). The luminal sides of non-permeable barriers were exposed separately to various EV strains, the infected barriers were incubated for the indicated times, and permeability was determined at each time p.i. (see below). The yield of infectious particles and the total amount of viral genome released through the abluminal and luminal sides were determined as described above.

Lucifer Yellow permeability assay. The paracellular seal of the endothelial barrier was determined in triplicate by testing the permeability to the Lucifer Yellow marker (LY, Sigma). The cell monolayers were washed twice with collecting buffer consisting of HBSS (GE Healthcare Life Science) supplemented with 1% of HEPES (GE Healthcare Life Science) and 1% of sodium pyruvate (GE Healthcare Life Science). The LY marker (50 µM; 400 µl) was added to the upper chamber. Cells were incubated at 37°C (5% CO_2 and 100% humidity) in three successive collecting wells, each containing 1.6 ml of collecting buffer, for respectively 10, 15, and 20 min. The LY concentration in the collecting buffer of each well and the stock LY solution were determined by fluorometry. Parallel negative control tests were performed with cell-free collagen-coated culture membranes. Samples were analysed in black 96-well microtiter plates using a Fluoroskan Ascent FL fluorometer (Thermo Electron Corporation, France) at 485 and 538 nm wavelengths for excitation and emission, respectively.

Scanning and transmission electron microscopy (SEM and TEM). The endothelial barriers were washed with 0.2M Na cacodylate buffer (NCB; pH 7.4) and fixed overnight at 4°C in 1.6% glutaraldehyde-NCB. The cells were fixed for 1 h with 1% OsO_4 in NCB. For SEM preparation, cells were dehydrated in graded ethanol, followed by critical point drying

with 100% ethanol and hexamethyldisilasane (1:1) for 10 min, sputter-coated with gold (JEOL JFC-1300), and observed at 5kV with a JEOL 6060-LV microscope. For TEM preparation, cells were dehydrated in graded ethanol, infiltrated sequentially with three mixtures of ethanol/EPON resin (2:1, 1:1, and 1:2) for 1 h each, embedded in EPON resin overnight at room temperature, and cured 2 days in a 60°C oven. Thin sections (70 nm, UC6 ultramicrotome, Leica) were stained with uranyl acetate and Pb citrate, and observed at 80 kV with a Hitachi H-7650 microscope. All chemical products were provided by Delta Microscopies.

Statistical Analysis. Statistical analyses were made with software Stata (version 12, StataCorp, College Station, US). Tests were two-sided, with a type I error set at a=0.05. Quantitative data are expressed as means (and associated standard deviation, Gaussian distribution verified by the Shapiro-Wilk test). Correlated data were analysed by mixed models to study the evolution of parameters taking into account between and within strain variability (random effects such as intercept and slope). These analyses were completed by ANOVA for repeated measures followed by post-hoc Tukey-Kramer test. Principal component analysis was done to explore the relation between several quantitative parameters. Correlation coefficients (Pearson or Spearman when appropriate) were calculated to quantify these relations.

LEGENDS TO FIGURES

Fig. 1. Heterogeneity of enterovirus infection in hCMEC/D3 cells. Replication in hCMEC/D3 cells of EV strains selected among species, types, and genogroups was examined at 24 h p.i. (a) Data are represented as means of two independent assays and given as the number of viral genome copies per cell (x-axis) and of infectious particles per cell (y-axis). Correlation between the yield of virus genome and yield of infectious virus is indicated. (b) Replication kinetics of virus strains of four EV types in hCMEC/D3 cells. Data are representative of means of three independent replicates for each virus E-30 (●), E-6 (▲), E-12 (♦), and EV-A71 (×). (c) Susceptibility spectrum of the hCMEC/D3 cell line to EVs estimated as the proportion of infected cells at 6 h p.i. A sample of 24 viral strains representing 19 different types was tested. Green and blue fluorescence indicate the VP1 protein and the nuclei, respectively. Scale bar, 100 µm. Data are represented as mean ± SD of three experiments. (d) Comparison of cell mortality rates at 24 h p.i. (n=15 EV strains). Data are represented as mean ± SD of four independent experiments. The blue line indicates the cell mortality rate (10%) in mock-infected cells (NoV).

Fig. 2. Principal component analysis of enterovirus replication in hCMEC/D3 cells. Ordination of the data obtained for 15 EV strains using principal component analysis. The horizontal axis is linked to cell sensitivity to EVs and the vertical axis to virus production.

Fig. 3. Disruption of a microvascular endothelial barrier during enterovirus infection. Endothelial barriers of hCMEC/D3 cells produced on Transwell® membranes were infected with E-6/CF2660-01 (a), E-11/CF228046-07 (b), E-12/CF1157-91 (c), E-30/CF2575-00 (d), EV-71/CF166105-10 (e), and EV-A71/CF160019-10 (f). At the indicated time points, the culture mediums in the luminal and abluminal compartments were collected and stored

separately. Paracellular permeability was measured. Data are indicated as mean ± SD of three experiments. The number of EV genome copies and infectious virus particles are respectively indicated with white and light grey bars for the luminal compartment, and respectively with dark grey and dashed bars for the abluminal compartment. Permeability coefficients for mock infected and infected barriers are indicated with green and red lines, respectively.

Fig. 4. Disruption of endothelial barriers during enterovirus infection. The hCMEC/D3 barriers were analysed with SEM at 24 h p.i. Representative fields of duplicate experiments are shown: mock-infected monolayers (a–c), and barriers infected with E-6/CF2660-01 (d–f), E-12/CF1157-91 (g–i), E-30/CF2575-00 (j–l), and EV-A71/CF166105-10 (m–o). White arrow head, breach of the endothelial barriers; red and green arrow heads, cells with a necrotic and an apoptotic shape, respectively; blue arrow head, round cell with no sign of altered plasma membrane.

Fig. 5. Ultrastructural features at 24 h p.i. of hCMEC/D3 barriers infected with an E-6 strain. The infected hCMEC/D3 barriers were observed at low magnification with TEM (a and b). Virus-induced reorganization of cytoplasmic elements (c). Features of the vesicular structures (d). Dense electron punctuation suggestive of virus aggregates (e). Bars, 4 µm (a and b); 500 nm (c–e). Representative fields of duplicate experiments are shown; mock-infected cells are shown in figure S4. Abbreviations: N, nucleus; M, mitochondria; MC, membranous replication complex; A, autolysosome/amphisome; V, virus aggregates.

Fig. 6. Ultrastructural features at 24 h p.i. of hCMEC/D3 barriers infected with an EV-A71 strain. The infected hCMEC/D3 barriers were analysed at low magnification with TEM; unaltered cells (a and b) and altered cells with virus-induced vesicular structures (c and d).

Features of the vesicular structures (e–i). Bar, 10 µm (a–d); 1 µm (e and f); 500 nm (g–i). Representative fields of duplicate experiments are shown; mock-infected cells are shown in figure S4. Abbreviations: N, nucleus; M, mitochondria; MC, membranous replication complex.

Fig. 7. The actin cytoskeleton network is disrupted in enterovirus-infected hCMEC/D3 cells. The hCMEC/D3 cells were analysed at 6 h p.i. during replication of strains E-12/CF1157-91 (a–c), E-6/CF2660-01 (d–i), E-30/CF2575-00 (j–l), E-11/CF228046-07 (m–o), and EV-A71/CF166105-10 (p–r); mock-infected cells (s–u). Actin network is shown in red, VP1 capsid protein in green, and nuclei in blue. Bars represent 10 µm. White arrow heads indicate intermediate disruption of actin cytoskeleton.

Fig. 8. Perinuclear relocation of active mitochondria in enterovirus-infected hCMEC/D3 cells. The hCMEC/D3 cells were analysed at 6 h p.i. during replication of E-12/CF1157-91 (a–c), E-6/CF2660-01 (d–f), E-30/CF2575-00 (g–i), E-11/CF228046-07 (j–l), and EV-A71/CF166105-10 (m–o); mock-infected cells (s–u). Active mitochondria are shown in red, VP1 capsid protein in green, and nuclei in blue. Bars represent 10 µm. White and yellow arrow heads indicate dense clusters and intermediate clustering of mitochondria, respectively.

ACKNOWLEDGEMENTS

The authors acknowledge the technical contribution of Gwendoline Jugie, Nathalie Rodde, and Isabelle Simon for helpful assistance in virus culture and sequencing. We thank Mr. Jeffrey Watts for help with preparing the English manuscript. Fluorescence confocal microscopy observations were done at the ICCF (Imagerie Confocale de Clermont-Ferrand) Centre, France. TEM and SEM observations were done at the Centre d'Imagerie Cellulaire Santé (Clermont-Ferrand, France).

REFERENCES

Agol, V. I. & Gmyl, A. P. (2010). Viral security proteins: counteracting host defences. *Nat Rev Microbiol* **8**, 867–878.

Antona, D., Lévêque, N., Chomel, J. J., Dubrou, S., Lévy-Bruhl, D. & Lina, B. (2007). Surveillance of enteroviruses in France, 2000-2004. *Eur J Clin Microbiol Infect Dis* **26**, 403–412.

Bailly, J. L., Chambon, M., Peigue-Lafeuille, H., Laveran, H., De Champs, C. & Beytout, D. (1991). Activity of glutaraldehyde at low concentrations (less than 2%) against poliovirus and its relevance to gastrointestinal endoscope disinfection procedures. *Appl Environ Microbiol* **57**, 1156–1160.

Belov, G. A., Nair, V., Hansen, B. T., Hoyt, F. H., Fischer, E. R. & Ehrenfeld, E. (2012). Complex dynamic development of poliovirus membranous replication complexes. *J Virol* **86**, 302–312.

Bergelson, J. M., Chan, M., Solomon, K. R., St John, N. F., Lin, H. & Finberg, R. W. (1995). Decay-accelerating factor (CD55), a glycosylphosphatidylinositol-anchored complement regulatory protein, is a receptor for several echoviruses. *PNAS (USA)* **91**, 6245–6248.

Bergelson, J. M., St John, N., Kawaguchi, S., Chan, M., Stubdal, H., Modlin, J. & Finberg, R. W. (1993). Infection by Echoviruses 1 and 8 Depends on the cx2 Subunit of Human VLA-2. *J Virol* **67**, 6847–6852.

Bozym, R. A., Morosky, S. A., Kim, K. S., Cherry, S. & Coyne, C. B. (2010). Release of intracellular calcium stores facilitates coxsackievirus entry into polarized endothelial cells. *PLoS Pathog* **6**, e1001135.

Conaldi, P. G., Serra, C., Mossa, A., Falcone, V., Basolo, F., Camussi, G., Dolei, A. & Toniolo, A. (1997). Persistent infection of human vascular endothelial cells by group B coxsackieviruses. *J Infect Dis* **175**, 693-696.

Chen, C. S., Yao, Y. C., Lin, S. C., Lee, Y. P., Wang, Y. F., Wang, J. R., Liu, C. C., Lei, H. Y. & Yu, C. K. (2007). Retrograde axonal transport: a major transmission route of enterovirus 71 in mice. *J Virol* **81**, 8996–9003.

Cheng, H. Y., Huang, Y. C., Yen, T. Y., Hsia, S. H., Hsieh, Y. C., Li, C. C., Chang, L. Y., & Huang, L. M. (2014). The correlation between the presence of viremia and clinical severity in patients with enterovirus 71 infection: a multi-center cohort study. *BMC Infect Dis* **14**, 417.

Coyne, C. B., Kim, K. S. & Bergelson, J. M. (2007). Poliovirus entry into human brain microvascular cells requires receptor-induced activation of SHP-2. *EMBO J* **26**, 4016–4028.

Eberle, K. E., Nguyen, V. T. & Freistadt, M. S. (1995). Low levels of poliovirus replication in primary human monocytes: possible interactions with lymphocytes. *Arch Virol* **140**, 2135-2150.

Engelhardt, B. & Coisne, C. (2011). Fluids and barriers of the CNS establish immune privilege by confining immune surveillance to a two-walled castle moat surrounding the CNS castle. Fluids and Barriers of the CNS **8**, 4.

Gromeier, M., & Wimmer E. (1998). Mechanism of injury-provoked poliomyelitis. J Virol **72**, 5056–5060.

Haddad, A., Nokhbeh, M. R., Alexander, D. A., Dawe, S. J., Grisé, C., Gulzar, N. & Dimock, K. (2004). Binding to decay-accelerating factor is not required for infection of human leukocyte cell lines by enterovirus 70. *J Virol* **78**, 2674-2681.

Khetsuriani, N., Lamonte-Fowlkes, A., Oberste, S. & Pallansch, M. A. (2006). Centers for Disease Control and Prevention. Enterovirus surveillance-United States, 1970-2005. *MMWR Surveill Summ* **55**, 1–20.

Kim, S., Kim, H. Y., Lee, S., Kim, S. W., Sohn, S., Kim, K. & Cho, H. (2007). Hepatitis B virus x protein induces perinuclear mitochondrial clustering in microtubule- and Dynein-dependent manners. *J Virol* **81**, 1714–1726.

Khong, W. X., Yan, B., Yeo, H., Tan, E. L., Ng, J. K. W., Chow, V. T. & Alonso, S. (2012). A non-mouse-adapted enterovirus 71 (EV71) strain exhibits neurotropism, causing neurological manifestations in a novel mouse model of EV71 infection. *J Virol* **86**, 2121–2131.

Lancaster, K. Z., & Pfeiffer, J. K. (2010). Limited trafficking of a neurotropic virus through inefficient retrograde axonal transport and the type I interferon response. *PLoS Pathog* **6**, e1000791.

Liang, C. C., Sun, M. J., Lei, H. Y., Chen, S. H., Yu, C. K., Liu, C. C., Wang, J. R., & Yeh TM. (2004). Human endothelial cell activation and apoptosis induced by enterovirus 71 infection. *J Med Virol* **74**, 597-603.

Limpens, R. W., van der Schaar, H. M., Kumar, D., Koster, A. J., Snijder, E. J., van Kuppeveld, F. J. & Bárcena, M. (2011). The transformation of enterovirus replication structures: a three-dimensional study of single- and double-membrane compartments. *MBio* **2**, 00166–11.

Merilahti, P., Koskinen, S., Heikkilä, O., Karelehto, E. & Susi, P. (2012). Endocytosis of integrin-binding human picornaviruses. *Adv Virol* **2012**, 547530.

Nishikawa, M., Matsubara, T., Yoshitomi, T., Ichiyama, T., Hayashi, T. & Furukawa, S. (2000). Abnormalities of brain perfusion in echovirus type 30 meningitis. J Neurol Sci **179**, 122 – 126.

Ohka, S., Nihei, C., Yamazaki, M. & Nomoto, A. (2012). Poliovirus trafficking toward central nervous system via human poliovirus receptor-dependent and –independent pathway. *Frontiers Microbiol* **2012**, 00147.

Rotbart, H. A. (1995). Meningitis and encephalitis. In Human enterovirus infections, pp 271-289. Edited by H. A. Rotbart. Washington D. C., ASM Press.

Ren, R. & Racaniello, V. R. (1992). Poliovirus spreads from muscle to the central nervous system by neural pathways. *J Infect Dis* **166**, 747–752.

Rojo, G., Chamorro, M., Salas, M. L., Viñuela, E., Cuezva, J. M. & Salas, J. (1998). Migration of mitochondria to viral assembly sites in African swine fever virus-infected cells. *J Virol* **72**, 7583–7588.

Sabin, A. B. (1956). Pathogenesis of poliomyelitis; reappraisal in the light of new data. *Science* **123**, 1151-1157.

Saijets, S., Ylipaasto, P., Vaarala, O., Hovi, T., & Roivainen, M. (2003). Enterovirus infection and activation of human umbilical vein endothelial cells. *J Med Virol* **70**, 430-439.

Spindler, K. R. & Hsu, T. H. (2012). Viral disruption of the blood-brain barrier. *Trends Microbiol* **20**, 282–290.

Stamatovic, S. M., Sladojevic, N., Keep, R. F. & Andjelkovic, A. V. (2012). Relocalization of junctional adhesion molecule A during inflammatory stimulation of brain endothelial cells. *Mol Cell Biol* **32**, 3414–3427.

Tabor-Godwin, J. M., Ruller, C. M., Bagalso, N., An, N., Pagarigan, R, R., Harkins, S., Gilbert, P. E., Kiosses, W. B., Gude, N. A., Cornell, C. T. & other authors (2010). A novel population of myeloid cells responding to coxsackievirus infection assists in the dissemination of virus within the neonatal CNS. J Neurosci **30**, 8676–8691.

Verma, S., Kumar, M., Gurjav, U., Lum, S., Nerurkar, V. R. (2010). Reversal of West Nile virus-induced blood-brain barrier disruption and tight junction proteins degradation by matrix metalloproteinases inhibitor. *Virology* **397**,130-138.

Verma, S., Lo, Y., Chapagain, M., Lum, S., Kumar, M., Gurjav, U., Luo, H., Nakatsuka, A. & Nerurkar, V. R. (2009). West Nile virus infection modulates human brain microvascular endothelial cells tight junction proteins and cell adhesion molecules: Transmigration across the in vitro blood-brain barrier. *Virology* **385**, 425-433.

Volle, R., Bailly, J. L., Mirand, A., Pereira, B., Marque-Juillet, S., Chambon, M., Regagnon, C., Brebion, A., Henquell, C. & other authors (2014). Variations in cerebrospinal fluid viral loads among enterovirus genotypes in patients hospitalized with laboratory-confirmed meningitis due to enterovirus. *J Infect Dis* **210**, 576–584.

Volle, R., Nourrisson C., Mirand, A., Regagnon, C., Chambon, M., Henquell, C., Bailly, J. L., Peigue-Lafeuille, H. & Archimbaud, C. (2012). Quantitative real-time RT-PCR assay for research studies on enterovirus infections in the central nervous system. *J Virol Methods* **185**, 142–148.

Vuorinen, T., Vainionpää, R., Vanharanta, R. & Hyypiä, T. (1996). Susceptibility of human bone marrow cells and hematopoietic cell lines to coxsackievirus B3 infection. *J Virol* **70**, 9018-9023.

Wahid, R., Cannon, M. J. & Chow, M. (2005a). Virus-specific CD4+ and CD8+ cytotoxic T-cell responses and long-term T-cell memory in individuals vaccinated against polio. *J Virol* **79**, 5988-5995.

Wahid, R., Cannon, M. J. & Chow, M. (2005b). Dendritic cells and macrophages are productively infected by poliovirus. *J Virol* **79**, 401-9.

Weksler, B., Romero, I. A. & Couraud, P. O. (2013). The hCMEC/D3 cell line as a model of the human blood brain barrier. *Fluids Barriers CNS* **10**, 16.

Weksler, B., Subileau, E. A., Perrière, N., Charneau, P., Holloway, K., Leveque, M., Tricoire-Leignel, H., Nicotra, A., Bourdoulous, S. & other authors (2005). Blood-brain barrier-specific properties of a human adult brain endothelial cell line. *FASEB J* **19**, 1872–1874.

Yang, W. X., Terasaki, T., Shiroki, K., Ohka, S., Aoki, J., Tanabe, S., Nomura, T., Terada, E., Sugiyama, Y. & Nomoto, A. (1997). Efficient delivery of circulating poliovirus to the central nervous system independently of poliovirus receptor. *Virology* **229**, 421–428.

Yen, M. H., Tsao, K. C., Huang, Y. C., Huang, C. G., Huang, Y. L., Lin, R., Chang, M. L., Huang, C. C., Yan, D. C., & Lin, T. Y. (2007). Viral load in blood is correlated with disease severity of neonatal coxsackievirus B3 infection: early diagnosis and predicting disease severity is possible in severe neonatal enterovirus infection. *Clin Infect Dis* **44**, e78–81.

Ylipaasto, P., Eskelinen, M., Salmela, K., Hovi, T. & Roivainen, M. (2010). Vitronectin receptors, αv integrins, are recognized by several non-RGD-containing echoviruses in a continuous laboratory cell line and also in primary human Langerhans' islets and endothelial cells. *J Gen Virol* **91**, 155–165.

Zanone, M. M., Favaro, E., Conaldi, P. G., Greening, J., Bottelli, A., Perin, P. C., Klein, N. J., Peakman, M. & Camussi, G. (2003). Persistent infection of human microvascular endothelial cells by coxsackie B viruses induces increased expression of adhesion molecules. *J Immunol* **171**, 438–446.

Zhang, Y., Cui, W., Liu, L., Wang, J., Zhao, H., Liao, Y., Na, R., Dong, C., Wang, L. & other authors (2011). Pathogenesis study of enterovirus 71 infection in rhesus monkeys. *Lab Invest* **91**, 1337–1350.

Figure

Click here to download Figure: 02_FIGURE_1_(04-02-2015).doc

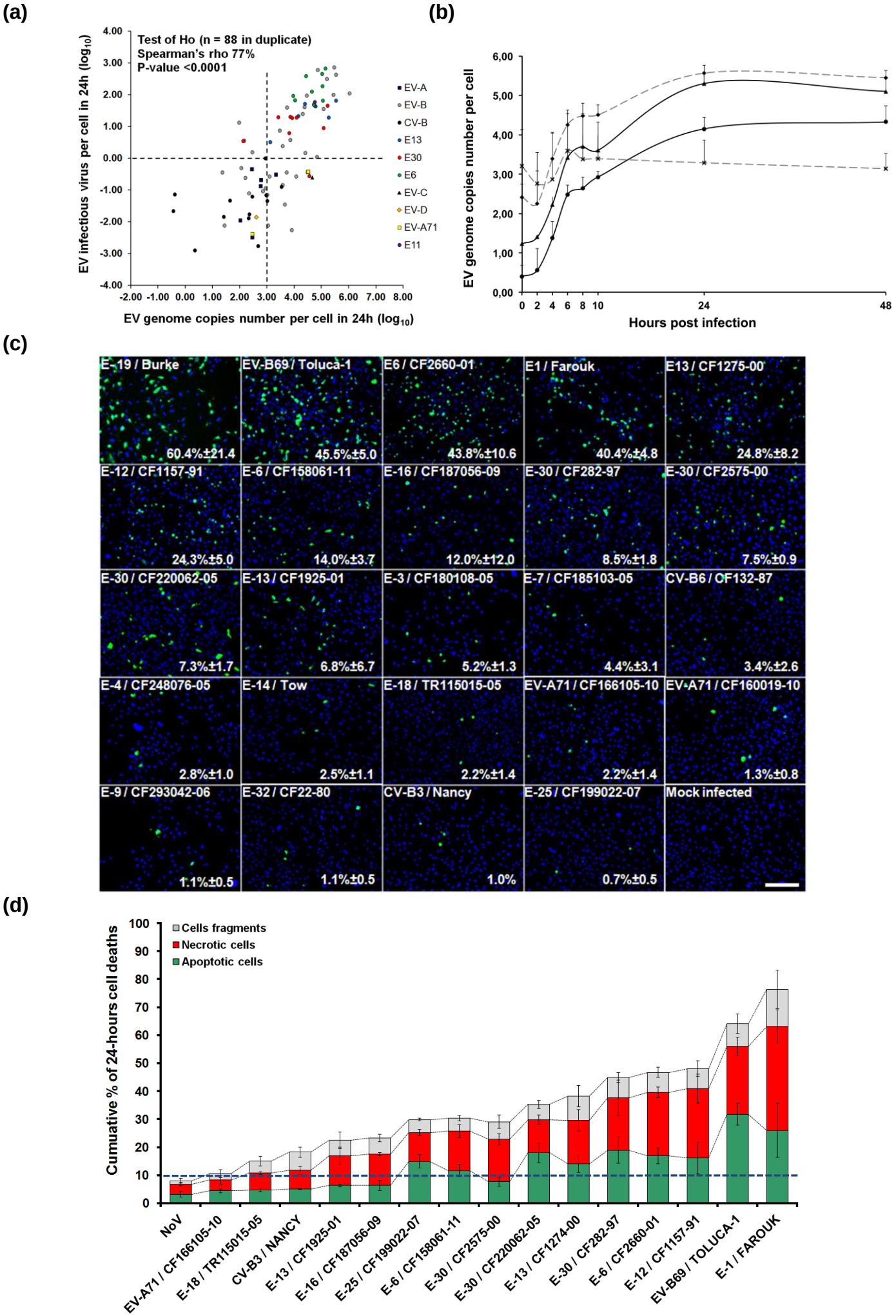

Figure
Click here to download Figure: 03_FIGURE_2.doc

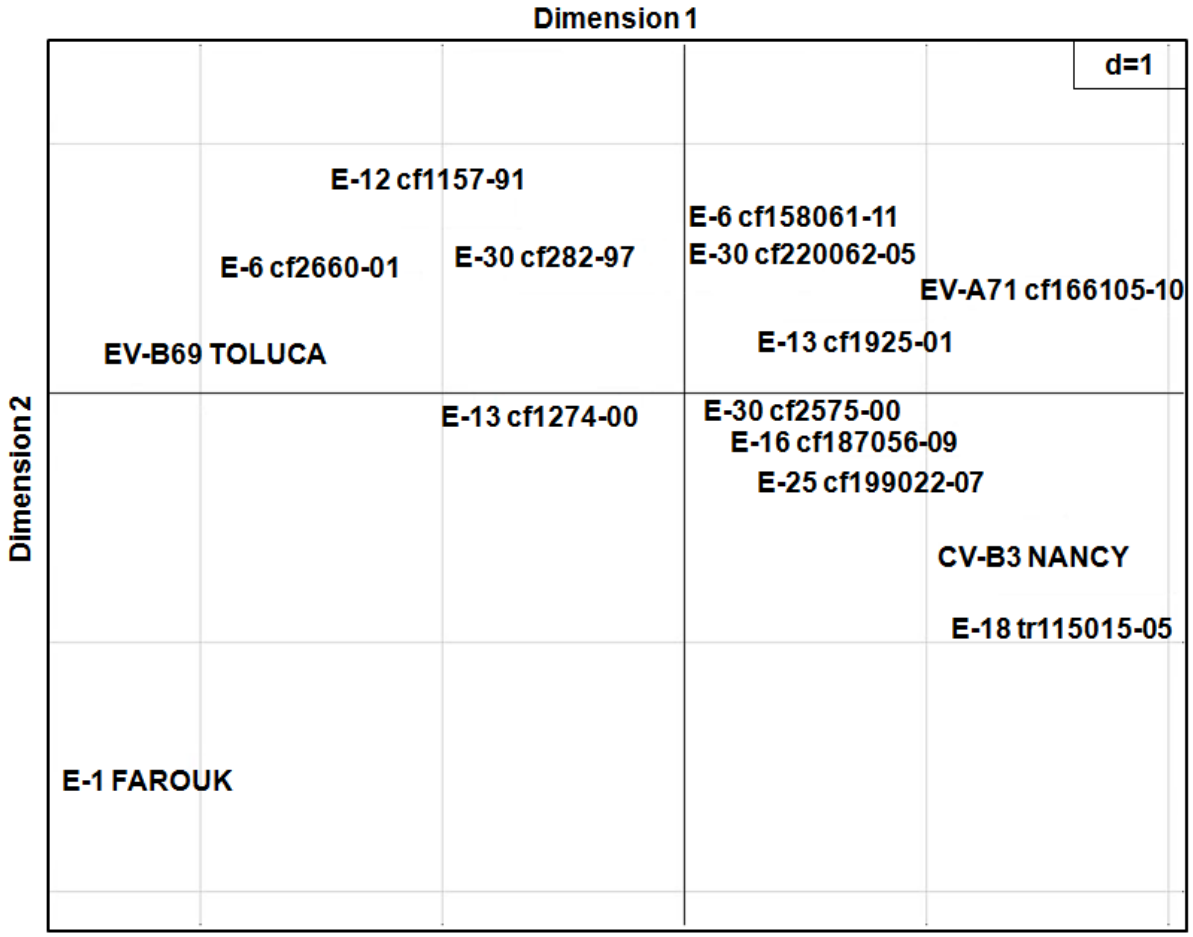

Figure
Click here to download Figure: 04_FIGURE_3_(04-02-2015).doc

Figure 3

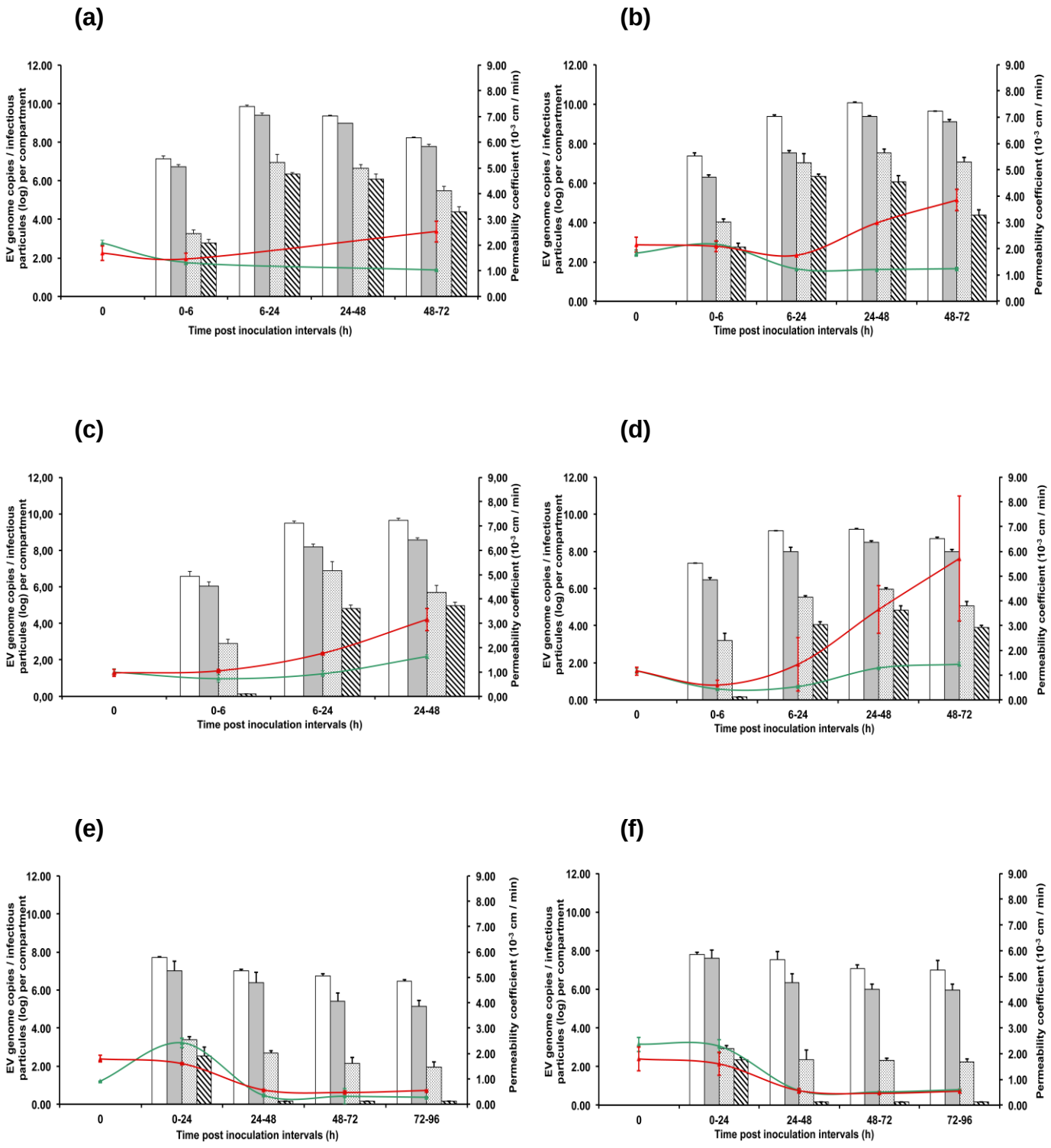

Figure
Click here to download Figure: 05_FIGURE_4.doc

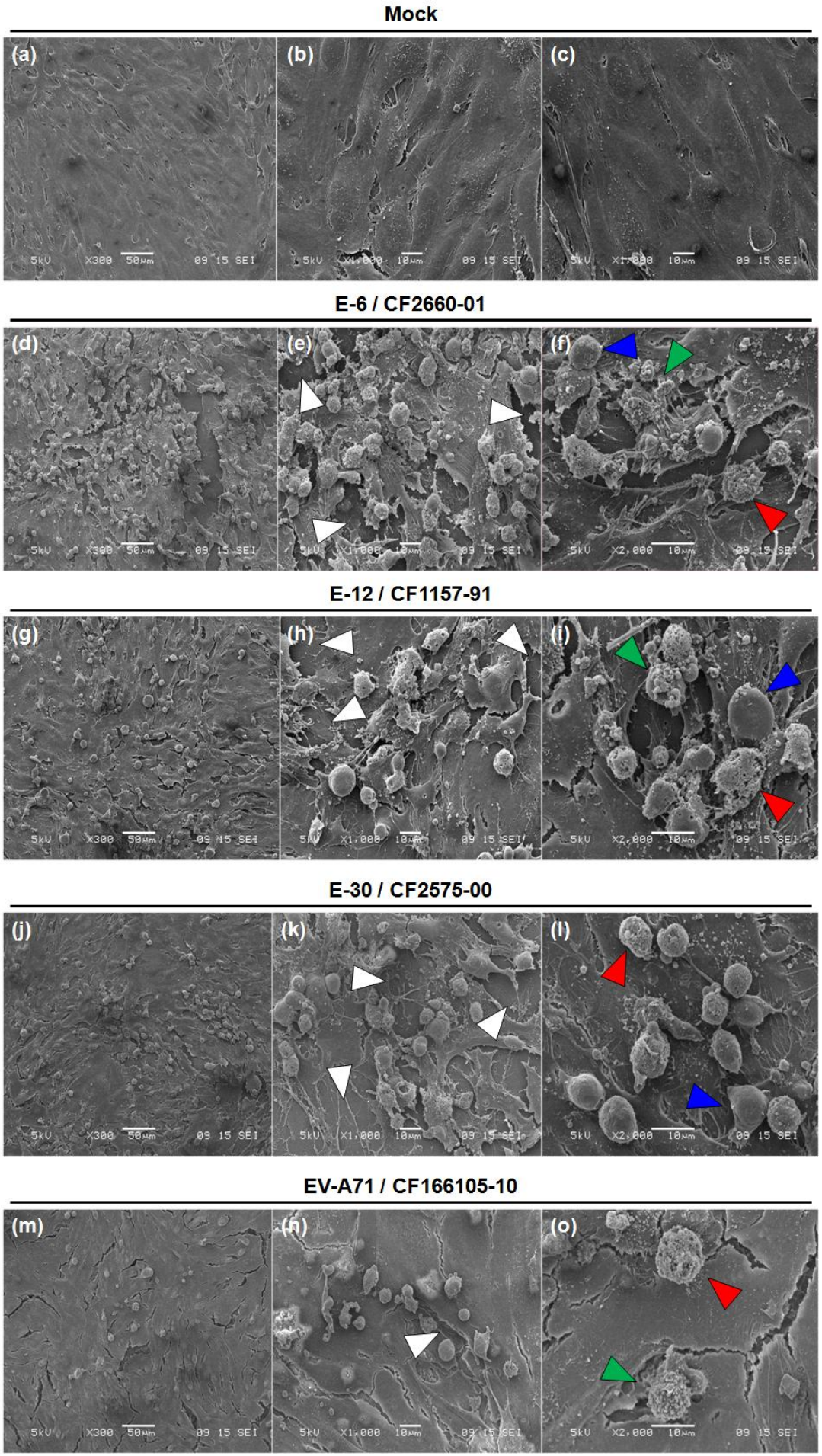

Figure
Click here to download Figure: 06_FIGURE_5.doc

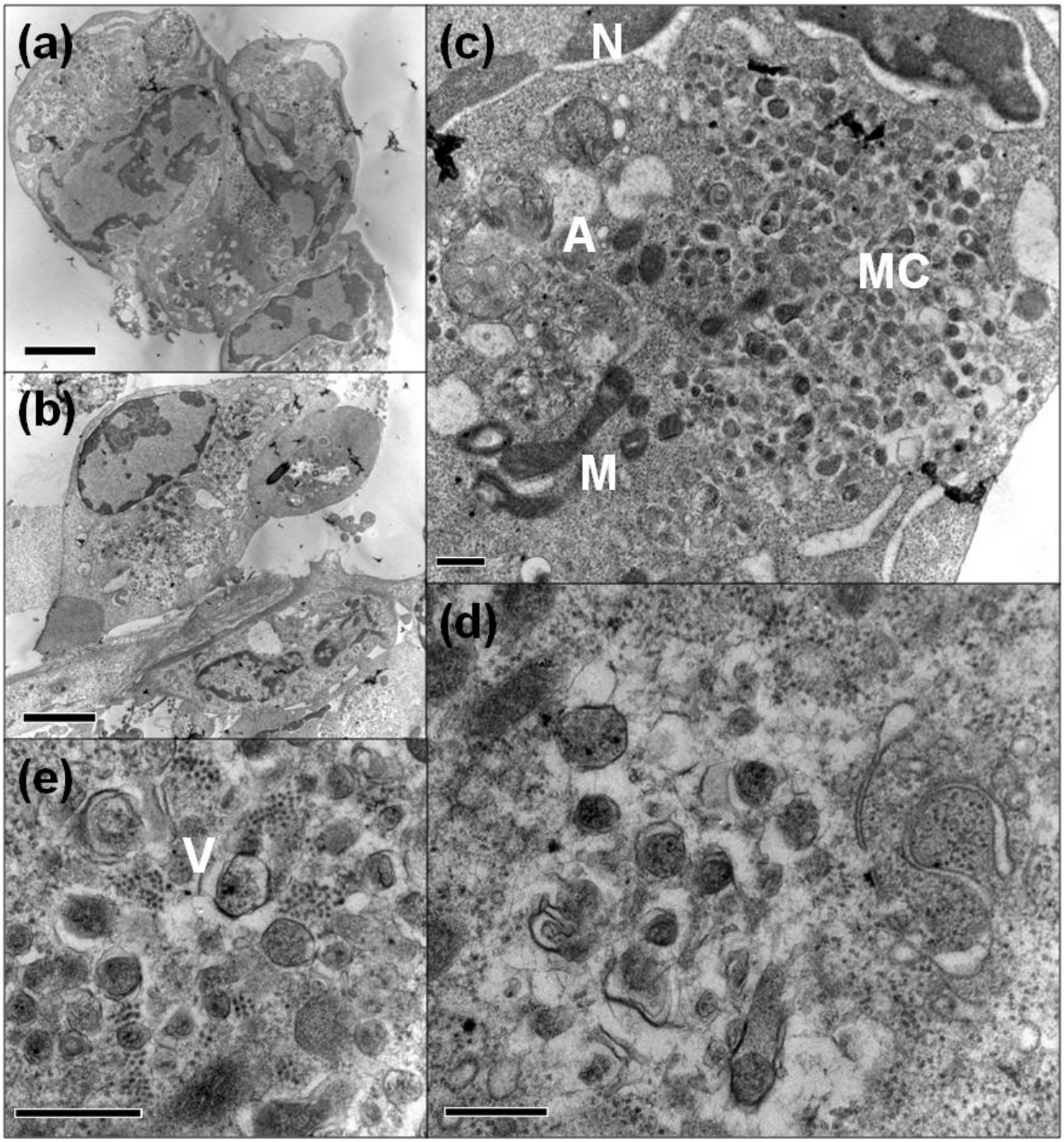

Figure
Click here to download Figure: 07_FIGURE_6.doc

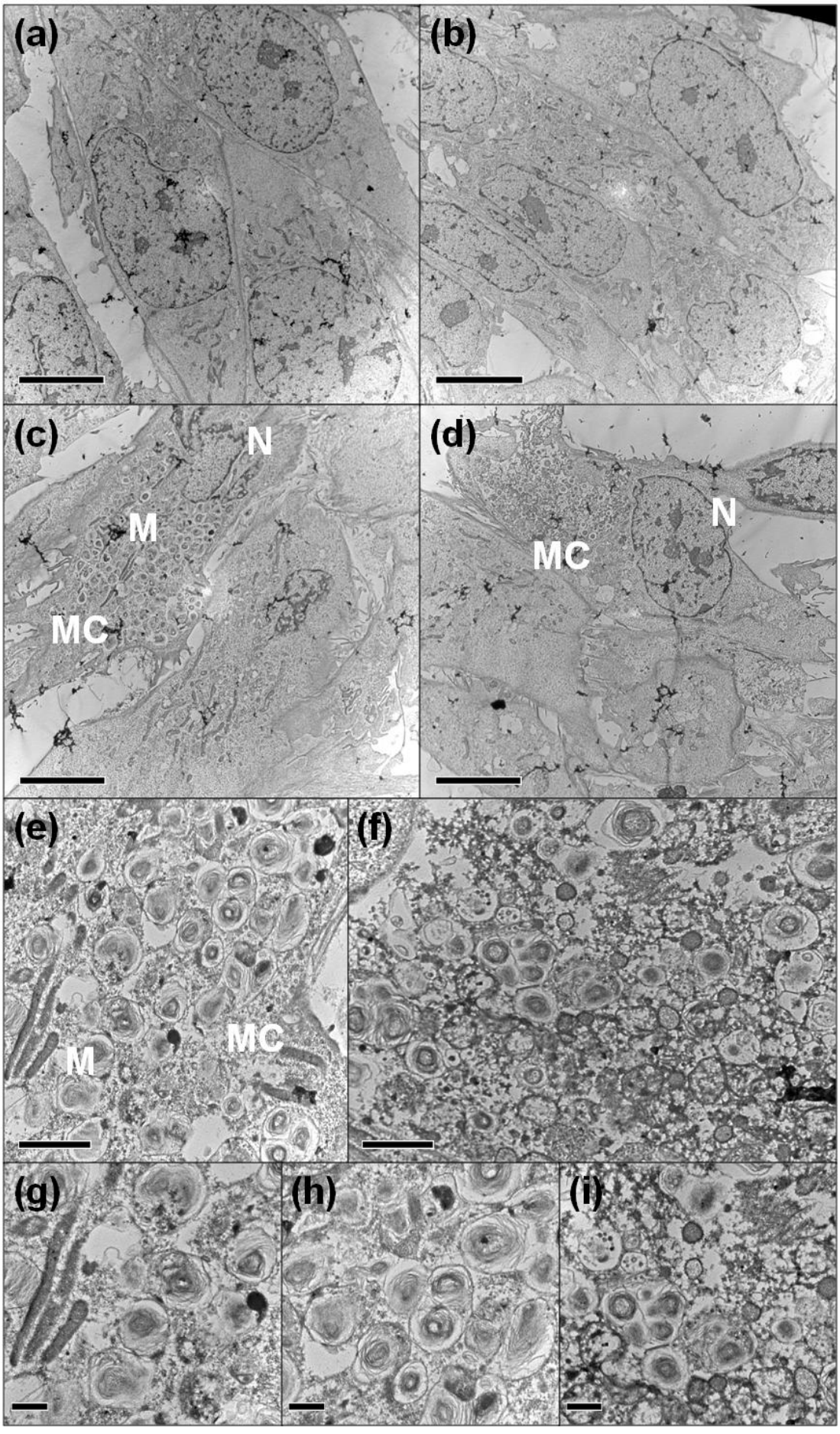

Figure
Click here to download Figure: 08_FIGURE_7.doc

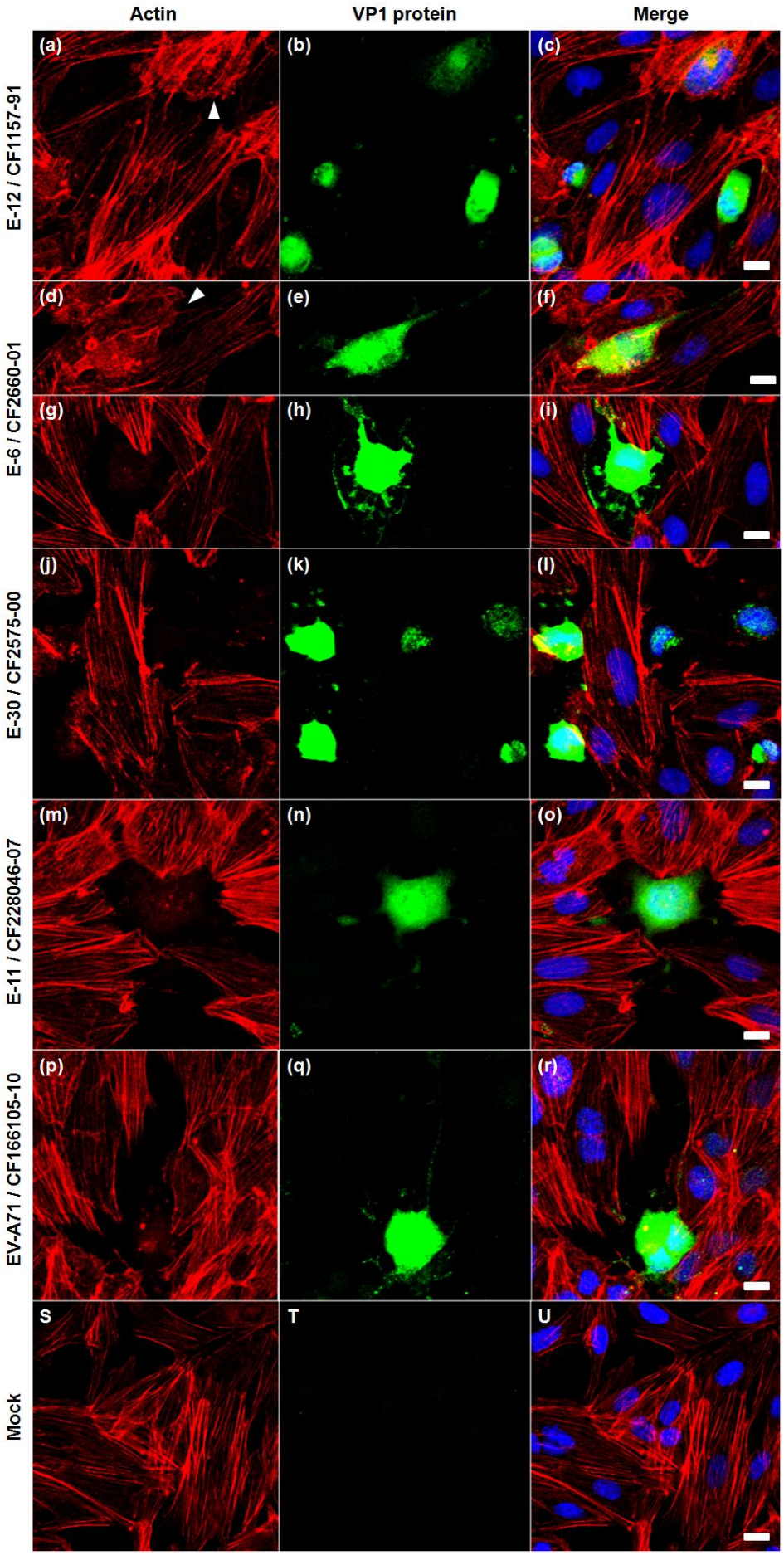

Figure
Click here to download Figure: 09_FIGURE_8.doc

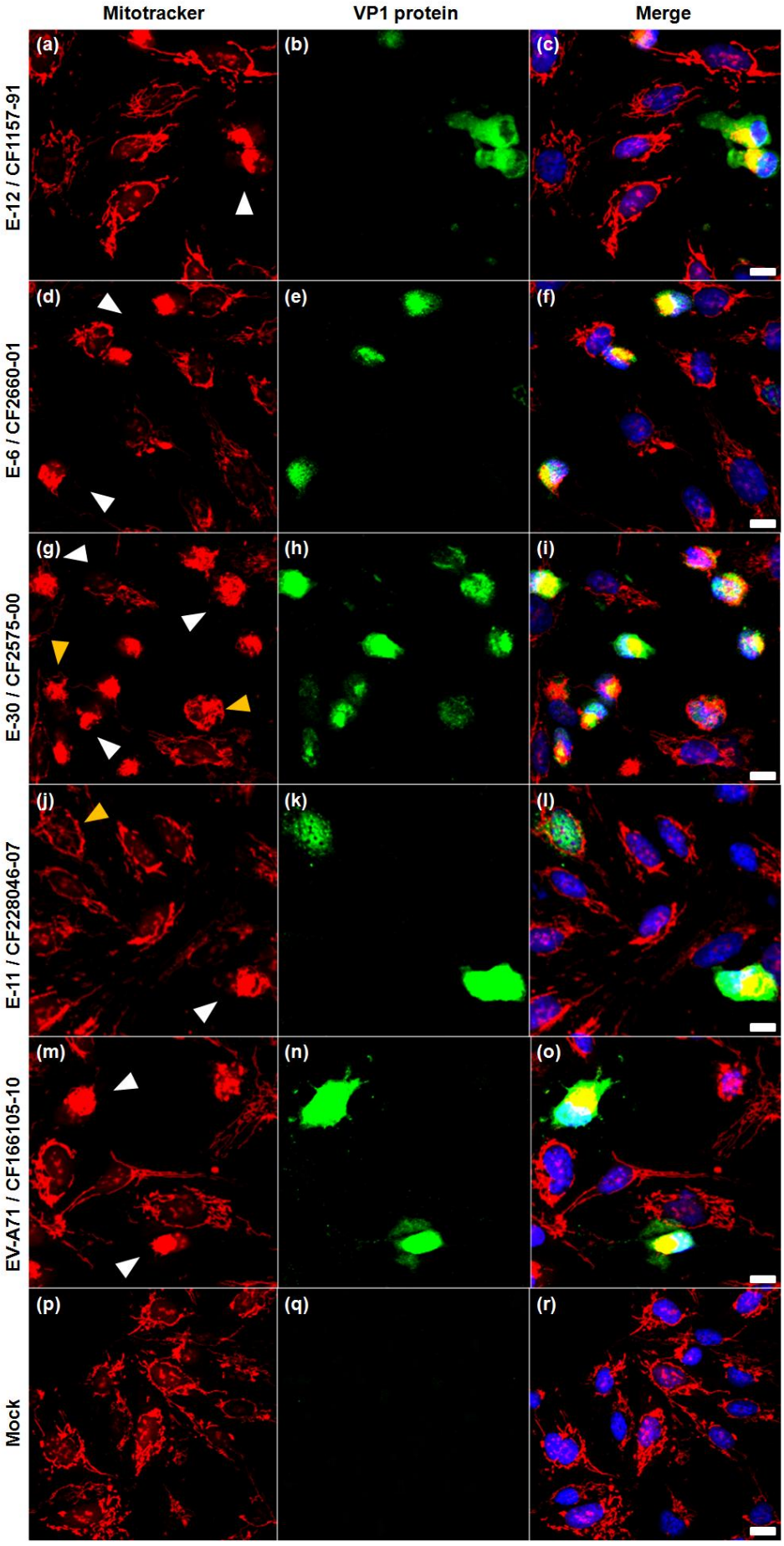

Supplementary Material Files

Click here to download Supplementary Material Files: Supplementary material.pdf